Electrostatic Interactions of Rodlike Polyelectrolytes with Repulsive, Charged Surfaces

David A. Hoagland

Department of Polymer Science and Engineering, University of Massachusetts, Amherst, Massachusetts 01003

Received April 4, 1989; Revised Manuscript Received December 1, 1989

ABSTRACT: The interactions of an isolated, rodlike polyelectrolyte with nearby surfaces of like charge are examined by using simple descriptions of both the polyelectrolyte and the free energy of interaction: the rodlike polymer is treated as a line charge and the interaction energy is handled in the Debye–Hückel approximation. A combination of electrostatic and entropic effects is predicted to produce both segmental depletion and chain orientation. The depletion predictions have been incorporated into a molecular model for polyelectrolyte separation in size exclusion chromatography columns containing a stationary phase with surface charge. In the region close to a flat wall, long-range repulsive interactions create preferential alignment of rod segments perpendicular to the plane of the wall; without these interactions, parallel alignment is favored.

Introduction

The behavior of polymers near nonadsorbing boundaries plays a key role in the numerous industrial and biological processes that confine dissolved polymer chains in spatially restricted geometries. Models for this behavior usually postulate that the polymer/surface interaction is totally steric—polymer chains are permitted to sample all configurations with equal probability except those that intersect a surface; intersecting configurations are completely disallowed. With steric effects dominant, a zone of diminished polymer concentration forms near each surface, and this zone has a characteristic dimension comparable to the radius of polymer chains in bulk solvent. This "depletion layer", first discussed by Asakura and Oosawa,[1] has its basis in configurational entropy, inasmuch as chains near the surface are limited to a reduced set of configurations as compared to chains far away. A decrease in the relative density of the low-entropy, surface-affected chains allows the system to equalize the chemical potential near the surface with that in the bulk solution. The extent of the density reduction depends on the distance from the surface, as the average chain entropy also varies with distance.

In water, with its high dielectric constant, both dissolved polymer chains and solution interfaces have a strong tendency to develop charge, either by ion adsorption or by dissociation of ionizable groups. Aqueous interfaces, in fact, are generally negatively charged, as are many polyelectrolytes of commercial interest. Such a combination of like charges can induce long-range repulsive forces between a dissolved polymer chain and nearby surfaces. From a technological standpoint these phenomena can significantly affect interpretation of size exclusion chromatography (SEC) data as well as implementation of oil recovery methods. In the latter instance, polymers used for mobility control may experience significant surface depletion due to the high surface charges of reservoir rock. When such conditions arise, the effective viscosity of the solution in the porous medium may be reduced due to the low viscosity of fluid layers near pore walls.

The electrostatic interactions between a charged polymer and a charged surface are "screened" by nearby ions in a way that can be predicted by the Poisson–Boltzmann equation. The thickness of the layer of diminished polymer concentration is therefore extremely sensitive to the ionic strength of the aqueous medium, with electrostatic contributions to this thickness minimized when a large excess of salts is added to the solution. In aqueous SEC of polyelectrolytes, for example, various review articles[2–4] suggest that addition of salts to raise the ionic strength to the level of 10^{-2}–10^{-3} M is sufficient to eliminate the electrostatic contributions to surface depletion. (The electrostatic interactions under discussion here are termed "ion exclusion" in the chromatography literature.) A chromatographic separation at high ionic strength depends only on molecular size and is independent of the ionic character of the chains; chromatographers nearly always seek this condition. In some SEC analyses, however, it is not possible to raise the ionic strength to this level, and the ionic strength is then observed to play a prominent role in determining the retention time of the various polymer fractions. Problems of this type occur, for example, when a polymer species (or any other mobile phase component) is not soluble at the high ionic strengths necessary to fully screen polymer/surface repulsion. We have frequently encountered this problem in our laboratories and, as a result, have been forced to conduct SEC experiments under operating conditions for which polymer retention is highly sensitive to ionic strength. Our difficulty in selecting appropriate experimental conditions to study such intractable polymers provoked the investigation reported in this contribution.

The interaction of flexible-coil molecules with nonadsorbing surfaces is complex even in the absence of long-range forces; as a result, many previous theoretical investigations of surface depletion have resorted to approximate numerical or analytical methods at the onset.[5–7] For rigid rodlike molecular models in dilute solution, on the other hand, the depletion layers formed near flat walls can be computed rather easily, and closed-form analytical solutions exist in simple geometries.[8–11] Rodlike molecules possess configurational entropy due to molecular rotation, and their depletion layers have the same qualitative features as those of flexible molecules. In our initial calculations we have therefore chosen to study a rodlike polyelectrolyte model in dilute solution, expecting that the results could be useful in studies of surface effects involving short DNA fragments or degraded xanthan fractions. This choice of a perfectly rigid molecular model has a significant drawback in that the molecular confor-

0024-9297/90/2223-2781$02.50/0

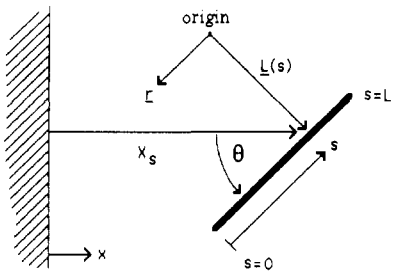

Figure 1. Sketch of the variables employed to define the rodlike polyelectrolyte's configuration relative to a neighboring surface.

mation is independent of ionic strength, an important if not dominant property of flexible polyelectrolytes. A few studies of polyelectrolytes near surfaces have retained chain flexibility, and the ensuing calculations are then both complex and approximate;[12,13] these studies have so far considered polymer/surface interactions only in the context of polymer adsorption. We find that the nonadsorbing rod problem can be done essentially analytically within the Debye–Hückel approximation for the electrostatic interactions. The present study can be regarded as an initial step in a broader investigation of how real, nonadsorbing polyelectrolytes respond to long-range surface forces.

The problems under investigation possess two or, in a few cases, three characteristic length scales. These are the rod length L, the Debye length κ^{-1}, and the width H of the pore (more precisely, a slit) containing the rod; this rod model assumes that the rod cross section is infinitesimal. The Debye length provides an estimate of the distance over which electrostatic repulsions are operative and may vary from 1 to 100 nm, depending on ionic strength. These distances are comparable to the persistence lengths l_p of many stiff polyelectrolytes (for double-stranded DNA, $l_p \sim 60$ nm; for xanthan or collagen $l_p \sim 120$–150 nm),[14] and this analysis is obviously valid only when L is somewhat less than l_p. The product $L\kappa$ controls much of the behavior to be described. When $L\kappa \gg 1$, the depletion layer will be dominated by entropic effects, and the depletion layer thickness will be equal to that of an uncharged rod. When $L\kappa \sim 1$, on the other hand, electrostatic effects may have a significant influence, particularly at large distances from the surface (i.e., at distances greater than L). When $L\kappa \ll 1$, the rod can be modeled as a point charge, and the depletion layer thickness will be approximately κ^{-1}. All three cases will be considered in the context of a single bounding wall against a semiinfinite solution reservoir and in a slit of finite width H; we will employ the slit calculations to provide a description of SEC separations involving rodlike polyelectrolytes. In addition to lowering concentration, the long-range interactions can modify the average relative orientation of rods with respect to the wall. This effect will be discussed, both with electrostatic effects present and in their absence; even in this latter case, literature results for surface-induced orientation have not been available.

The present calculations employ a line charge model for the polyelectrolyte chain, a model that has been amply discussed in the literature.[15–23] The simplifications made possible by ignoring the finite diameter of the polymer backbone are significant. Previous workers interested in the electrostatic interactions of rodlike polyelectrolyte segments in aqueous media have applied this simplification with considerable success, notably in models for the chain expansion and second virial coefficient of polyelectrolytes in dilute solution.[15–20] Ignoring the finite diameter of the polyelectrolyte is a good approximation (within the Debye–Hückel limit) except when the polymer–surface separation is comparable to the chain diameter. At such small length scales effects such as van der Waals interactions, hydration forces, and the location of charge groups in the repeat unit structure cannot be ignored; we will not incorporate any of these complications in the present model and will therefore focus only on the depletion effects arising from phenomena operative at length scales much greater than the chain diameter.

Model Formulation

1. Electrostatics. Using standard approximations,[24,25] one can obtain from solution of the full nonlinear Poisson–Boltzmann equation the electrostatic potential $\psi(\mathbf{r})$ for the combination of a line charge polyelectrolyte model and a flat wall

$$\nabla^2\psi(\mathbf{r}) = \frac{2zen_0}{\epsilon}\sinh\left[\frac{ze\psi(\mathbf{r})}{kT}\right] - \delta[\mathbf{r} - \mathbf{L}(s)]\frac{eL}{\epsilon l_c} \quad (1)$$

where ϵ is the permittivity of the fluid (assumed constant), z is the valence of the free ions, n_0 is the concentration of free ions in bulk solution, k is the Boltzmann constant, T is the temperature, and e is the charge of an electron. The polyelectrolyte rod is characterized by its length L and an average distance l_c between bound charges, each of magnitude e; the chain configuration is defined with respect to the origin of the $\mathbf{r}$ coordinate system through a vector function $\mathbf{L}(s)$. The following line integral is necessary to fully specify the rod configuration:

$$\int_{\mathbf{r}}\int_0^L \delta[\mathbf{r} - \mathbf{L}(s)]\, ds\, d\mathbf{r} = L \quad (2)$$

The scalar parameter s, specifying position along the rod backbone, runs from 0 to L, and δ is the usual Dirac delta function. The effective charge of the molecule has been smeared uniformly along its length; this approximation is not unduly severe for the current purposes, even when real chains with widely separated charges are considered. Constant surface charge boundary conditions are written

$$\frac{\partial\psi}{\partial x} = -\frac{\sigma}{\epsilon} \text{ at } x = 0 \quad (3)$$

$$\psi, \frac{\partial\psi}{\partial x} = 0 \text{ as } z \to \infty \quad (4)$$

where x is an independent variable specifying position relative to the surface, and σ is the surface charge density. The surface charge density can be alternatively expressed in terms of the surface potential ψ_0 when the rod is not present, $\sigma = (8n_0\epsilon kT)^{1/2}\sinh[ze\psi_0/2kT]$. The rod/surface geometry and associated coordinate notation are sketched in Figure 1.

The appropriate boundary conditions for the potential field during the approach of a real polyelectrolyte chain to a charged surface are certainly more complex than suggested by eq 3. A better description would stipulate a fixed density of ionizable groups on both the polymer chains and the surface and then allow the degree of dissociation of these groups to depend upon the local potential environment induced during the interaction. This approach, pioneered by Ninham and Parsegian,[26] requires information about the dissociation constants of a specific polyelectrolyte and a specific surface, details we wish to avoid here. Alternately, the surface potential could be held constant during the interaction, the assumption commonly imposed in models for closely approaching col-

loidal particles. For aqueous systems, however, in which surface charge is normally developed by dissociation of bound groups, the constant surface charge conditions is more satisfactory than the constant surface potential condition.[27] The neglect of the electrostatic field induced within the solid as the polyelectrolyte approaches the solid's charged surface can be justified whenever the dielectric constant of the solid material is small and the solid wall is thick.[28]

A general analytical solution of eq 1 in the presence of a charged wall appears a formidable challenge. Reduction of the nonlinear term via application of the Debye–Hückel approximation makes the problem much simpler, without eliminating the depletion and orientation effects under study. We therefore linearize the Poisson–Boltzmann equation as follows:

$$\frac{2zen_0}{\epsilon}\sinh\left[\frac{ze\psi(\mathbf{r})}{kT}\right] \cong \kappa^2\psi(\mathbf{r}) \tag{5}$$

where κ is the reciprocal of the Debye length

$$\kappa = \left[\frac{2e^2n_0z^2}{\epsilon kT}\right]^{1/2} \tag{6}$$

The Debye–Hückel approximation obviously restricts solution of the Poisson–Boltzmann equation to regions where the potential is small. The interaction free energy will be calculated by a method that imposes this restriction only at a dividing surface between the rod and the wall, not necessarily in the immediate proximity of either the rod or the wall where the potential can be large.

If $\psi(\mathbf{r})$ has been determined for a given rod/surface configuration by evaluating eqs 1–4, the relative electrostatic free energy ΔE of the rod (compared to the rod's electrostatic free energy in bulk solvent) can be calculated by integrating the work required to bring the rod charge into its specified configuration from some distant position at which the electrostatic potential is zero. There are several equivalent approaches to this problem, and the one we have selected is discussed extensively in the context of rod/rod interactions by Brenner and Parsegian[18] and in the context of sphere/sphere interactions by Bell et al.[29] and Oshima et al.[30] Basically, the electrostatic free energy is obtained as the integral of the line charge density multiplied by the potential exerted by the wall at each point occupied by the line charge.

$$\Delta E = \int_{\mathbf{r}}\int_0^L \psi_w(\mathbf{r})\frac{e}{l_c}\delta[\mathbf{r} - \mathbf{L}(s)]\, ds\, d\mathbf{r} \tag{7}$$

The potential in the aqueous solution induced by the wall charge, ignoring the presence of the line source, is denoted $\psi_w(\mathbf{r})$. Alternatively, ΔE is calculated as an integral over the product of the potential along the fluid boundary (induced by the line source in absence of the wall charge) and the surface charge density of the wall. The second approach is more difficult than the first, since the potential field of the arbitrarily placed line source must be solved in the presence of the dielectric discontinuity of the wall. The equivalency of the two approaches arises from the symmetry of the Green's function for a point source charge, in a medium of variable dielectric constant, as described by the linearized Poisson–Boltzmann equation. The line source rod model is then regarded as an integral over a uniform distribution of point sources.

The relationships of eq 7 to more commonly encountered forms for the free energy of interaction of charged bodies are given in Fixman.[24] The quantity ΔE comprises the only component of the system electrostatic energy needed to examine the equilibrium configurational statistics of the rod; it excludes the self-energy of the rod, ion atmosphere, and charged wall. These extra components of the free energy are independent of the rod/surface configuration and are therefore ignored. More generally, the total interaction energy between charged bodies includes osmotic contributions in addition to the screened charge interactions discussed so far. These interactions arise due to the deformation of the counterion cloud as one charged body approaches another; they create free energy changes even when one of the bodies is uncharged. As this model of the polyelectrolyte is a line rather than a cylinder, osmotic contributions to the interaction energy are absent; their neglect will only be important at separation distances of the order of the diameter of the rod. The sole condition for application of eq 7 is that the total potential at some stress surface lying between the rod and the wall can be expressed as the linear superposition of the individual potential field of a line source and a charged wall (recognizing, of course, that this wall separates domains of differing dielectric constant). Thus, the analysis will remain valid even for highly charged rods if the charge parameter used in eq 7 is the asymptotic long-range effective charge density for the line source (likewise for the wall if it is highly charged) and the rod/wall separation is somewhat greater than the inverse Debye length. At lower charge densities, where the potential is everywhere small, the actual charge density at the line source can be directly substituted into eq 7.

The rod's configurational partition function depends explicitly on the rod orientation, specified by generalized angular coordinates Ω, and the rod center-of-mass position x_c. Equations 1–7 must therefore be solved for each allowed configuration of the rod, taking care to skip any configuration violating the surface of a bounding wall. Following the Boltzmann distribution law, the relative concentration of each of the permitted rod/surface configurations, compared to the concentration of this configuration in free solution, can be expressed

$$\frac{f(\Omega,x_c)}{f_0} = e^{-\Delta E(\Omega,x_c)/kT} \tag{8}$$

In the absence of wall constraints or electrostatic potentials, the rod assumes all configurations with equal likelihood; in this case f_0 is independent of Ω and x_c. Near a surface, however, f_0 does depend on the rod/wall configuration.

James and Williams[31] recently presented a scheme for numerically solving the nonlinear Poisson–Boltzmann equation in nontrivial geometries. Specifically discussed is the potential field around an infinitely long, charged cylinder held at fixed separation from a charged, parallel wall; the cylinder's radius is comparable to the rod/wall separation. Even in this simple geometry the calculations are complex, strongly suggesting that a complete solution to the present problem (including finite length, nonparallel orientation, and nonlinear electrostatic effects) would be exceedingly painstaking. Such a solution would necessarily incorporate successive three-dimensional numerical integration of the nonlinear equation for $\psi(\mathbf{r})$ and evaluation of the electrostatic free energy of each of the permitted rod/surface configurations. The full nonlinear calculation is only necessary for highly charged rods at small distances from the wall (as in the case illustrated by James and Williams). These configurations are highly improbable, as their electrostatic energy is high, so they will have little impact on equilibrium configurational statistics. In any case, these configurations occur at such small separations that in real sys-

tems other surface forces probably dominate over electrostatic forces.

The approach outlined in previous paragraphs requires the solution of the Poisson–Boltzmann equation in the presence of charged fluid boundaries; the presence of the charged rod is specifically excluded from this solution. An accounting of the rod becomes necessary only as the free energy change is subsequently calculated. Potential fields induced by charged boundaries are discussed in elementary texts.[32] Near a single wall against a semi-infinite reservoir of fluid

$$\psi(x) = \frac{2kT}{ze} \ln\left[\frac{1 + \gamma \exp(-\kappa x)}{1 - \gamma \exp(-\kappa x)}\right] \tag{9}$$

where γ is given

$$\gamma = \frac{\exp[ze\psi_0/2kT] - 1}{\exp[ze\psi_0/2kT] + 1} \tag{10}$$

In a narrow slit of thickness H, the Debye–Hückel solution for ψ, valid everywhere in the slit when the surface potential is not too great, can be written

$$\psi = \psi_0 \frac{\cosh[\kappa(H/2 - x)]}{\cosh(\kappa H/2)} \qquad 0 < x < H/2,\ \psi_0 < ze/2kT \tag{11}$$

where ψ_0 is the surface potential; the surface charge is related to the surface potential as $\sigma = \kappa\epsilon\psi_0 \tanh(\kappa H/2)$. More general expressions for the electrostatic potential in the slit, valid at larger surface charge, could be employed as well,[33] at the expense of added calculational effort. We assume here, and later on, that the narrow channel opens to a reservoir in which the potential falls to zero and that the polymer concentration reaches its bulk solution value in this distant reservoir.

2. Entropic Effects. Depletion of concentration near a well for a rodlike polymer model was first discussed by Giddings et al.,[8] DiMarzio and Guttman,[34] and Casassa.[10] Later, this subject was more fully explored by Auvray.[9] Recently, Hoagland[11] presented a formalism for solving rod problems in constricted geometries, and his approach will be followed here. The first step is to divide the rod into two sections, a longer one of length λ_1 and a shorter one of length λ_2. The segment concentration profile as a function of distance from the wall is then written $C(\lambda_1,x)$, $L/2 < \lambda_1 < L$. Special quantities that can be derived from the function $C(\lambda_1,x)$ include the monomer concentration profile $C_m(x)$, the center-of-mass concentration profile $C(L/2,x)$, and the rod end concentration profile $C(L,x)$:

$$C_m(x) = \frac{2}{L}\int_{L/2}^{L} C(\lambda_1,x)\, d\lambda_1 \tag{12}$$

$$C(L/2,x) = \int_{L/2}^{L} \delta(\lambda_1 - L/2) C(\lambda_1,x)\, d\lambda_1 \tag{13}$$

$$C(L,x) = \int_{L/2}^{L} \delta(\lambda_1 - L) C(\lambda_1,x)\, d\lambda_1 \tag{14}$$

These quantities are easily calculated when rod entropy alone is important:

$$C_m(x) = x/L[1 - \ln(x/L)] \qquad 0 < x < L \tag{15a}$$

$$= 1 \qquad x > L \tag{15b}$$

$$C(L/2,x) = 2x/L \qquad 0 < x < L/2 \tag{16a}$$

$$= 1 \qquad x > L/2 \tag{16b}$$

$$C(L,x) = 0.5(x/L + 1) \qquad x < L \tag{17a}$$

$$= 1 \qquad x > L \tag{17b}$$

Each concentration profile has been normalized by its free solution value.

Integration of eqs 12–14 requires knowledge of $C(\lambda_1,x)$, a function that contains information about both entropy and enthalpy (when long-range interactions are included). The segment concentration profile $C(\lambda_1,x)$ can be determined by counting all permitted configurations with the point λ_1 on the rod fixed to position x; each configuration is then weighted according to its appropriate Boltzmann factor. The number of configurations for each (λ_1,x) pair is proportional to the area of the spherical envelope defined by rotation of the longer end of the rod about position x. Configurations that include wall violations by either the longer or shorter ends of the rod are disallowed. The following forms are obtained by this process if we avoid, for the slit problem, the less important case when $H < 2L$. In a very narrow slit where $H < 2L$, the rod, with segment λ_1 at fixed location x, can experience steric interactions with both bounding walls upon rotation; following ref 11, this problem is easily solved, but its solution introduces no additional physics. Strong electrostatic interactions with both walls, on the other hand, typically persist even when $H > 2L$.

$$C(\lambda_1,x) = \frac{1}{2}\int_{-x(L-\lambda_1)}^{x/\lambda_1} \exp(-\Delta E/kT)\, dy \qquad \lambda_1 < L - x \tag{18}$$

$$C(\lambda_1,x) = \frac{1}{2}\int_{-1}^{x/\lambda_1} \exp(-\Delta E/kT)\, dy \qquad \lambda_1 > L - x,\ \lambda_1 > x \tag{19}$$

$$C(\lambda_1,x) = \frac{1}{2}\int_{-1}^{1} \exp(-\Delta E/kT)\, dy \qquad \lambda_1 < x \tag{20}$$

The upper and lower limits on the integrals have been derived by accounting for the full range of accessible angles for each value of λ_1 and x; a more complete discussion of these limits is given in an earlier paper.[11]

3. Solution Method. The calculation of the rod/wall configurational statistics has been reduced to a series of nested integrals that can be evaluated easily by standard numerical techniques. The most significant problem is bookkeeping; to illustrate the necessary procedures we will discuss the calculation of the monomer concentration profile $C_m(x)$ near a single interacting wall. We first derive $C(\lambda_1,x)$, employing Figure 2 to help us properly account for the limits on the integral combinations derived from eqs 18–20. The resulting forms for $C(\lambda_1,x)$ are then inserted in eq 12, leading to three different expressions for monomer concentration $C_m(x)$, depending on the relative value of x to rod length L:

$$x < L/2$$

$$C(x) = \frac{1}{L}\int_{L/2}^{L-x}\int_{-x/(L-\lambda_1)}^{x/\lambda_1} \exp(-\Delta E/kT)\, dy\, d\lambda_1 + \frac{1}{L}\int_{L-x}^{L}\int_{-1}^{x/\lambda_1} \exp(-\Delta E/kT)\, dy\, d\lambda_1 \tag{21}$$

$$L/2 < x < L$$

$$C(x) = \frac{1}{L}\int_{L/2}^{x}\int_{-1}^{1} \exp(-\Delta E/kT)\, dy\, d\lambda_1 + \frac{1}{L}\int_{x}^{L}\int_{-1}^{x/\lambda_1} \exp(-\Delta E/kT)\, dy\, d\lambda_1 \tag{22}$$

$$x > L$$

$$C(x) = \frac{1}{L}\int_{L/2}^{L}\int_{-1}^{1} \exp(-\Delta E/kT)\, dy\, d\lambda_1 \tag{23}$$

The Boltzmann factor can be obtained by integrating along the rod backbone to obtain ΔE

$$\Delta E(\lambda_1,x,y) = \frac{e}{l_c}\int_0^L \psi(x_s)\, ds \tag{24}$$

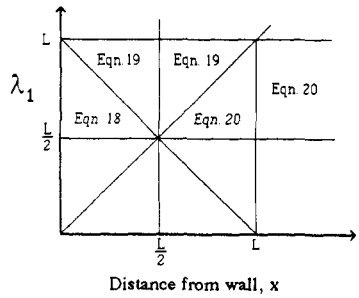

Figure 2. Sketch of the application range of each of eqs 18–20. The segmental concentration is determined by a vertical integration, at fixed x, over the range $L/2 < \lambda_1 < L$.

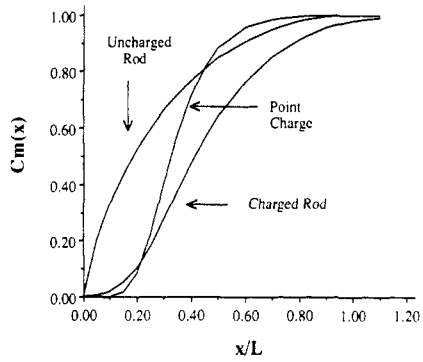

Figure 3. Monomer concentration profile near a single interacting wall along with that of an uncharged rod of equal length and that of a point charge of equal charge magnitude. ($Q^* = 10$, $L^* = 10$, $\psi^* = 2$.)

where all variables are as before, and x_s is the x coordinate of the local rod position variable s, $x_s = x - y(\lambda_1 - s)$. The dummy variable y can be identified as cos (θ), where the angle θ is defined in Figure 1.

Results will be presented in terms of a set of dimensionless variables: $Q^* = (L/l_c)(1/z)$ = dimensionless total rod charge, $L^* = \kappa L$ = dimensionless rod length, and $\psi^* = \psi_0 ze/kT$ = dimensionless surface potential. The required integrations are performed by using the trapezoidal rule, with an accuracy in the final, reported quantity better than ±1%.

Results

1. Concentration Profiles. For a typical set of parameter values ($Q^* = 10$, $L^* = 10$, $\psi^* = 2$), the concentration profiles for monomer and rod center-of-mass, $C_m(x)$ and $C(L/2,x)$, are illustrated in Figures 3 and 4, respectively. In each figure is shown, for comparison, the concentration profile $C_p(x)$ of a point charge possessing an equal total charge magnitude Q. Also displayed are the concentration profiles (of the appropriate type) for an uncharged rod of equal length L. The point charge concentration profile has been calculated from the Boltzmann law

$$C_p(x) = \exp(-Q\psi(x)/kT) \tag{25}$$

and the uncharged rod concentration profiles from eqs 15 and 16. It is clear from the figure that at this intermediate value of κL the concentration profiles for the charged rod polyelectrolyte model are a blend of the point charge and uncharged rod concentration profiles. For smaller κL ($\kappa L < 10$) the trend is toward greater similarity with the point charge profile, while at larger κL the trend is toward greater similarity with the uncharged rod profile. The upturn in the concentration profile of the charged rod model, at a distance approximately one Debye length from the wall, is rather abrupt, at least as compared with the upturn observed for an uncharged rod molecule of the same size.

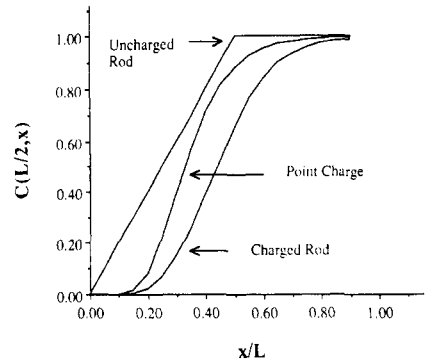

Figure 4. Center-of-mass concentration profile near a single interacting wall, alongside that of an uncharged rod of equal length and that of a point charge of equal charge magnitude, ($Q^* = 10$, $L^* = 10$, $\psi^* = 2$.)

The combination of charge and length effects is especially simple for the limiting case of small κL. In this situation a perturbation analysis shows that the monomer concentration profile near the wall can be expressed as a product of the point charge profile and uncharged rod profile (eqs 15 and 25, respectively)

$$C_m(x) = (x/L)[1 - \ln(x/L)] \exp[-Q\psi(x)/kT] \qquad x < L \tag{26}$$

Equation 26 provides a quantitative analytical description, according to comparison with the computational results, for $\kappa L \leq 1$.

2. Depletion Layer Thickness. The mixture of enthalpic and entropic exclusion effects for the charged rodlike polymer can be presented most simply in terms of a mean depletion layer thickness $\langle d \rangle$ (made dimensionless with L)

$$\langle d \rangle = \int_0^\infty [1 - C(\lambda_1,x)]\, dx \tag{27}$$

Inasmuch as the total number of each segment λ_1 over the domain $0 < x < \infty$ is independent of the choice of λ_1, the dimensionless mean depletion layer thickness is invariant to the specification of λ_1. Normally, eq 27 is most easily evaluated by using $\lambda_1 = L/2$. The value of $\langle d \rangle$ is 0.25 for the uncharged rod model.

The mean depletion layer thickness $\langle d \rangle$ is analogous to the excluded volume parameter appearing in theories for nonideal gases or in theories for polymer expansion in good solvents. Figure 5 displays the mean depletion layer thickness for a charged rod model with $Q^* = 10$ and $\psi^* = 2$; κL is a parameter. Also shown in the figure are the mean depletion layer thicknesses, under identical conditions, of a point charge and an uncharged rod. The point charge depletion thickness is given, in the Debye–Hückel limit, as $Q\psi_0\kappa^{-1}/kT$. Figure 5 reveals the expected result that the charged rod undergoes a smooth transition from behavior similar to that of a pointlike charge at low κL to that of an uncharged rod at high κL. Significantly, this transition occurs gradually with κL, persisting over an order-of-magnitude span of this parameter. Similar behavior is seen at other values of rod charge Q^* and surface potential ψ^*, as illustrated in Figure 6 and 7. Several optical techniques may give direct experimental access to the mean depletion layer thickness for polyelectrolyte solutions above surfaces with known surface potential (evanescent wave-induced fluorescence[35] or evanescent wave ellipsometry,[36] for example). A simpler way to study concentration depletion near surfaces, however, is to measure the partitioning of model poly-

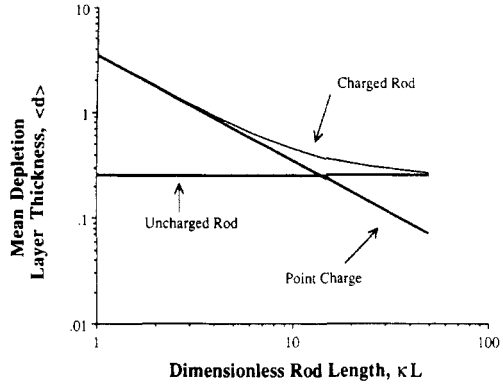

Figure 5. Mean depletion layer thickness as a function of dimensionless rod length. For comparison, the limiting forms for an equivalent point charge and an equivalent uncharged rod are also displayed. ($Q^* = 10$, $\psi^* = 2$.)

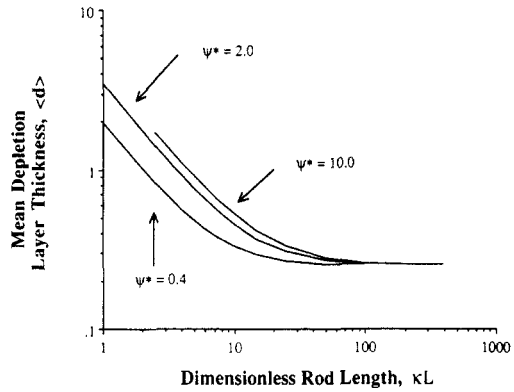

Figure 6. Mean depletion layer thickness as a function of dimensionless rod length; the dimensionless surface potential ψ^* is the parameter. ($Q^* = 10$.)

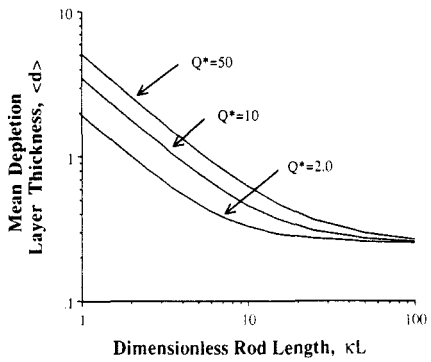

Figure 7. Mean depletion layer thickness as a function of the dimensionless rod length; the dimensionless charge Q^* of the rod is the parameter. ($\psi^* = 2$.)

electrolytes between a thin channel and a large, connected reservoir; this technique is discussed in a later section.

3. Orientation. The reduction of configurations by entropic and enthalpic interaction with an impenetrable wall alters not only the local segmental concentrations but also the position-dependent orientational distribution function of the rodlike molecule. This alteration occurs even in the absence of long-range forces when the rod/wall interaction is entirely steric. Such orientational effects can be presented in terms of an orientational order parameter S defined with respect to a normal vector for the wall:

$$S = \frac{3\langle \cos^2 \theta \rangle - 1}{2} \tag{28}$$

The averaging process denoted $\langle\ \rangle$ is to be executed, at least initially, with respect to the concentration-weighted orientations of all the rod segments λ_1 located at position x. By analogy to eq 12 and to eqs 18–20

$$\langle \cos^2 \theta \rangle = \frac{\int_{L/2}^{L} \theta(\lambda_1,x)\, d\lambda_1}{\int_{L/2}^{L} C(\lambda_1,x)\, d\lambda_1} \tag{29}$$

where

$$\theta(\lambda_1,x) = \frac{1}{2}\int_{-x/(L-\lambda_1)}^{x/\lambda_1} y^2 \exp(-\Delta E/kT)\, dy \qquad \lambda_1 < L - x \tag{30}$$

$$\theta(\lambda_1,x) = \frac{1}{2}\int_{-1}^{x/\lambda_1} y^2 \exp(-\Delta E/kT)\, dy \qquad \lambda_1 > L - x,\ \lambda_1 > x \tag{31}$$

$$\theta(\lambda_1,x) = \frac{1}{2}\int_{-1}^{1} y^2 \exp(-\Delta E/kT)\, dy \qquad \lambda_1 < x \tag{32}$$

Perfect ordering parallel to the wall yields $S = -1/2$, while complete random ordering, always obtained far from the wall, provides $S = 0$. In the limit of perfect rod alignment perpendicular to the wall, $S = 1.0$.

Without rod/wall electrostatic interactions the order parameter is easily obtained by analytical integration of eqs 30–32 with $\Delta E = 0$.

$$S = \frac{1 - (x/L)^2 + 2\ln(x/L)}{4 - 4\ln(x/L)} \tag{33}$$

The function S is plotted in Figure 8 for both the charged and uncharged rod models. The x/L intercept of S is $-1/2$ for the uncharged rod, although the evolution of S toward this value is masked in the figure since the abscissa is linear in x/L. That the orientation function reaches $-1/2$ at its intercept implies that the contributions to S at this point from rod end segments, those with $\lambda_1 = L$, are overwhelmed by the contributions from middle segments associated with rods that are actually laying flat against the wall. This prediction is not obvious since $C(\lambda,1x)$ is 0.0 at $x = 0$, except for the case $\lambda_1 = L$. The contribution from the end segments rises very rapidly away from $x = 0.0$, explaining the rapid evolution of S at small x/L. At larger x/L the orientation function increases to its isotropic limit over a length scale comparable to the length of the rod.

When electrostatic interactions are included, the functional dependence of S on x/L is immediately altered since the configurations with the rod laying flat against the wall present a prohibitive energetic cost. The rod segments found near the wall are now mainly contributed by rods with centers-to-mass at larger x/L. Rotation of these rods by Brownian motion is responsible for bringing the few segments near the wall into other loca-

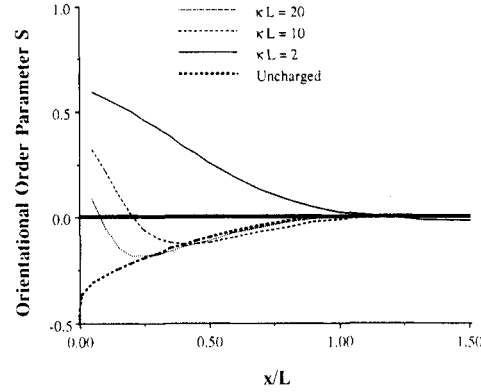

Figure 8. Orientational order parameter S. The dimensionless rod length L^* is the parameter. ($Q^* = 10$, $\psi^* = 2$.)

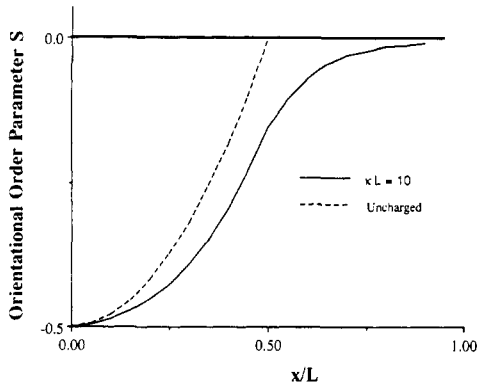

Figure 9. Orientational order parameter defined by alignment of rod center of mass. Compared to the segmental-based orientation functions of the previous figure, this orientation function increases monotonically with distance away from the wall until reaching its plateau value. ($L^* = 10$, $Q^* = 10$, $\psi^* = 2$.)

tions. The average orientation near the wall is therefore nearly perpendicular to the wall. With inclusion of electrostatic interactions S goes through a minimum at $\kappa x \sim 1$; this minimum occurs in the same range of x/L as does the upturn in the monomer concentration profile.

If orientation is examined as a function of center-of-mass position, the orientation function S monotonically increases from $-1/2$ at the wall toward its asymptotic random value of zero in free solution. The expected trend is displayed in Figure 9. The averaging process is now over center-of-mass rod segments alone; this average can be obtained by weighting the integrand of eq 29 with $\delta(\lambda_1 - L/2)$. The monotonic increase shown by this new average simply reflects the necessary ordering by the wall, irrespective of long-range interaction, of rods with center-of-mass positions closer to the wall than L. An experiment to measure wall ordering will mostly likely be sensitive to the monomer-based orientation discussed in the previous paragraph, not that associated with the center of mass. Many probes of surface structure are sensitive to segmental structural anisotropy near the surface (IR-ATR, X-ray reflectance, ellipsometry), so experimental verification of these predictions appears possible. In the dilute regime, of course, effects arising from molecular orientation are small and perhaps difficult to measure. It would therefore be interesting and worthwhile to extend these results to nondilute concentrations.

4. Partition Coefficients. The reduction in polymer concentration near surfaces implies that the average concentration of rodlike polyelectrolytes in small pores will be less than in free solution. For a slit of width H this reduction can be expressed in terms of the partition coefficient K_p

$$K_p = \frac{2}{H}\int_0^{H/2} C(L/2,x)\, dx \tag{34}$$

remembering that $C(L/2,x)$ has been normalized with respect to its free solution value outside the slit. It is worth noting that the partition coefficient conveys the same information as the mean depletion layer thickness $\langle d \rangle$ only when the depleted zone is confined to a region near the wall of thickness less than $H/2$; this condition will generally not be satisified when electrostatic effects are included, as these effects persist over several multiples of the Debye length into the solution. For an uncharged rod of length L (with $H > L/2$)

$$K_p = 1 - L/2H \tag{35}$$

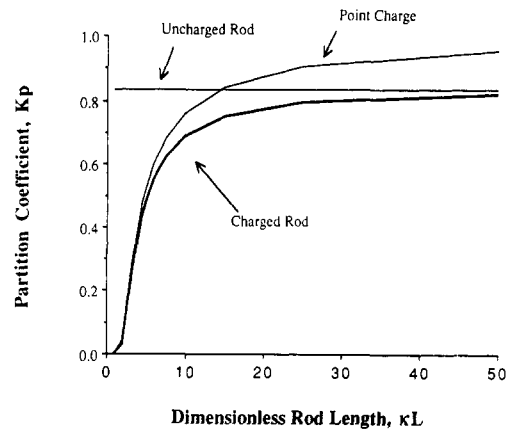

Figure 10. Variation of partition coefficient with κL, holding L constant. This figure can be interpreted in terms of changes in ionic strength ($\kappa \sim I^{1/2}$) at fixed rod length. For small l the partition coefficient of the rod is comparable to that of a point charge, while at larger l, the behavior is more comparable to that of an uncharged rod model. ($Q^* = 10$, $\psi^* = 2$, $H = 3L$).

while for a point charge Q, using eq 11

$$K_p = 1 - \frac{20Q\psi_0}{(\kappa H)kT}\tanh\frac{\kappa H}{2} \tag{36}$$

in the Debye–Hückel limit.

The partition coefficient for the charged rod model as a function of κL is shown in Figure 10, with $Q^* = 10$, $W^* = 2$, and $H = 3L$. Varying κL under these conditions is equivalent to holding L constant and varying κ. At low κ (equivalently, at low ionic strength) the charged rod behaves as a point charge and is highly excluded from the slit by electrostatic repulsion. At much higher κ the electrostatic interactions are reduced, and the rod enters the pore in a fashion more closely approaching that of an uncharged rod. It is important to note, however, that even at $\kappa L = 40$ the effects of ionic strength are still significant. Smith and Deen[37] have commented on the remarkable persistence of electrostatic effects at high ionic strength when charged spheres are partitioned between bulk solution and highly confining cylindrical pores of like charge; in the case of spherical particles, of course, the electrostatic effects include an osmotic component.

5. Implications for SEC of Polyelectrolytes. Partition coefficients provide information directly relevant to polymer size analysis in SEC columns. The elution volume of a polymer fraction V_r is related to the partition coefficient through the expression[38]

$$V_r = V_e + K_p V_s \tag{37}$$

where V_e is the column exclusion limit and V_s is the permeation volume of solvent in the stationary phase. We will discuss a sample case in which the dimensionless surface potential $\psi^* = 2$ and the rodlike polyelectrolyte is 10 nm long, possessing one fully dissociated valence 1 ionic group per nanometer; this charge density is below the limits of charge density predicted by "counterion condensation".[39,40] For this rod specification the product κL exceeds 40, the critical threshold for neglect of electrostatic effects under the conditions of the previous section, only when the ionic strength exceeds 1.4 M. The Poisson–Boltzmann equation has little theoretical foundation at such a high ionic strength, of course, but an appropriate electrostatic theory for high ionic strength solutions has yet to be derived. With this caveat, it appears reasonable to interpret the results of Figure 10 as indicating that electrostatic depletion will be significant at ionic strengths less than the general range 0.5–1.5 M. The

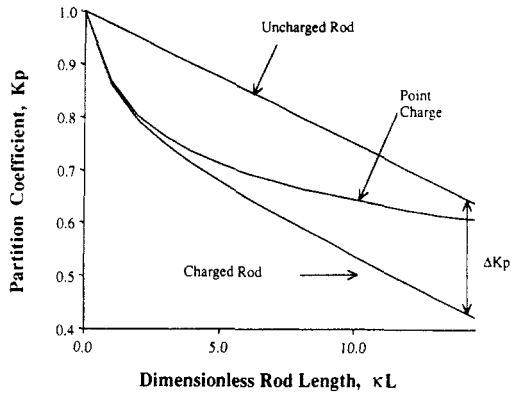

Figure 11. Variation of partition coefficient with κL, holding κ constant. This figure can be interpreted in terms of the rod length dependence of partitioning at fixed ionic strength. The parameter ΔK_p is defined as the difference between the charged rod partition coefficient and the uncharged rod partition coefficient after this difference has become constant at large κL. ($\kappa H = 20$, $\psi^* = 2$, $Q^* = L^*$.)

SEC implications are obvious—electrostatic depletion of highly charged, rodlike macromolecules from surfaces cannot be neglected except at large values of ionic strength, values that are much above than commonly practiced. In fact, this exercise considered a polymer of rather low charge density; electrostatic depletion effects in real systems are likely to be greater.

With acceptance that electrostatic effects are significant, the most important model prediction for SEC applications is the dependence of the electrostatic depletion on molecular length L, at fixed ionic strength and rod charge density; such constraints are the ones pertinent to a molecular weight analysis. These conditions are obtained when κH is constant ($\kappa H \gg 1$), as is Q/L (the charge per unit length). Figure 11 shows how the partition coefficient depends on chain length holding these parameters constant. The very shortest rods are excluded from the slit by electrostatic effects alone. Larger rods are excluded by both electrostatic and entropic effects. Significantly, the dependence of K_p on L follows the same functional dependence on L, at large L, as for uncharged rods; the parameter ΔK_p defined in the figure is essentially constant when $\kappa L > 1$. This parameter does depend on the rod's charge density and the stationary phase surface potential as revealed in the following correlation of the partition coefficient:

$$K_p = 1 - \frac{L}{2H} - \frac{\kappa^{-1}}{2H} f(Q/L,\psi_0) \qquad \kappa L \gg 1, \quad H \gg L \qquad (38)$$

The third term provides a quantitative correlation of ΔK_p under the conditions noted.

The physical interpretation of eq 38 is simple. At finite ionic strength the effective channel width to a charged molecule is reduced by an amount proportional to κ^{-1}. Similarly, the effective length of the charged rod is increased by an amount proportional to κ^{-1}. Inasmuch as the rod lengths under consideration are smaller than the channel width, the rod length effect dominates the ionic strength dependence of K_p. Equation 38 is therefore written so that the electrostatic effect appears as a rod length increase proportional to κ^{-1}. Nicolai and Mandel[20] have used a similar length increase argument to partially explain the ionic strength dependence of the second virial coefficient of short DNA fragments, and Munch et al.[41] have applied this argument to membrane rejection of polyelectrolytes. These partition coefficient predictions can be directly tested by conducting SEC experiments with either ionic strength or pore size as the variable.

The impact for SEC is now clear—although electrostatic effects are important to separation of charged rods, as long as the rod lengths exceed the Debye length κ^{-1}, the relative separation of rods can be interpreted in terms of rod molecular weight alone. This is true even when the actual retention of the various polymer fractions depends strongly on ionic strength. Since the rod model does not incorporate polyelectrolyte expansion, it is not certain if these statements will apply to flexible polymer chains. Further calculations for flexible polymer models are clearly warranted.

Although experimental data enabling a rigorous verification of this model have yet to appear in the literature, the problem of polyelectrolyte partitioning into charged pores has been a subject of both theoretical and experimental study.[37,41-45] In all theoretical analyses the polymer has been modeled either as an impenetrable rigid sphere or as a permeable porous sphere. Model predictions have been compared to partitioning data for rigid protein molecules, flexible polyelectrolytes, and colloidal lattices. Similarly, configurational effects on membrane filtration have been examined by Long et al.[46] using tobacco mosaic virus as a model rodlike macromolecule. Experimental efforts have not yet addressed both configurational and electrostatic effects in a rodlike system.

Limitations of the Model

Three major conditions must be satisfied before applying this model: the polyelectrolyte must be truly rodlike, the rod diameter should be small, and the potential on a stress surface between the polyelectrolyte and the wall must be expressible as a sum of the individual potentials of the polyelectrolyte and the wall. The first condition is satisified for polymers such as DNA and xanthan if the chain length is sufficiently short compared to the persistence length. For the polymers cited, the persistence length is at least 50 times the chain radius. It is thus possible to study chains that are both rigid and possess a high aspect ratio.

Electrostatic effects are affected to some degree by the finite radius of polymer chains. This influence can be understood by examining the expression for the radial dependence of the potential around a charged cylinder of radius r_0

$$\psi(r) = \left(\frac{2kT}{e}\right)\frac{X(r)K_0(\kappa r)}{\kappa r_0 K_1(\kappa r_0)} \qquad (39)$$

where K_0 and K_1 are the modified Bessel functions, and $X(r)$ plays the role of an effective charge density at radial distance r. In the Debye–Hückel limit $X(r)$ is a constant equal to the real linear charge density evaluated at the rod surface. The rod radius enters the Debye–Hückel potential expression only through the parameter combination $\kappa r_0 K_1(\kappa r_0)$, which tends toward unity for small κr_0. Even for the largest reasonable value of κr_0 (≈ 0.1) this product is within 2% of its limiting value. The rod radius is thus a negligible parameter in the electrostatic free energy calculation until the rod/wall separation is of the order of r_0. At these smaller separations electrostatically induced osmotic forces, van der Waals interactions, and hydration forces will all be significant.

The third condition for applying the model, the existence of a stress surface on which the potential is expressible as a linear superposition of individual potentials, will be automatically obeyed if the Debye–Hückel approximation is valid everywhere between the polymer and the

wall. This validity occurs when the wall charge density is low and the polymer linear charge density is not too high. From the calculations of Le Bret and Zimm,[47] Fixman,[24] and Russel,[17] the potential around a cylindrical polyelectrolyte is found to be everywhere expressible through the linearized Poisson–Boltzmann equation under the following conditions:

$$l_c \gtrsim 2l_b, \quad l_b = e^2/\Delta kT \tag{40}$$

In this case the charge density parameter $X(r)$ is constant. We therefore expect that the Debye–Hückel approximation is valid if the average distance on the chain between covalently bound, fully ionizable, valence 1 ionic groups is at least 1.4 nm (the Bjerrum length l_b is about 0.7 nm in water). At higher charge densities the asymptotic long-range effective charge density $X(\infty)$, provided by models such as the counterion condensation theory of Manning,[39] will be adequate to characterize the polymer's charge density if the smallest distance between the polyelectrolyte rod and the wall is of order magnitude κ^{-1} or greater. At smaller separations and at higher charge densities the interaction between polyelectrolyte and wall can only be determined by complete evaluation of the boundary value problem posed in eq 1, with subsequent evaluation of ΔE through a charging process.[32] It appears that such elaboration is not useful since other forces are likely to dominate when the necessary conditions for this more complex calculation arise.

Conclusions

A simple model of the interaction of a charged, rodlike polymer and nearby charged surfaces has been formulated. The simplest test of this model will be provided by measurements of the ionic strength dependence of SEC elution of monodisperse rodlike polyelectrolytes such as DNA or xanthan; such data can then be compared to eq 38. This experiment would be useful in verifying that size separation can occur, and be interpreted as such, even when electrostatic effects are important. Direct depletion layer measurements by optical methods would also be helpful. Important theoretical extensions of this work will be to examine flexible polyelectrolyte models in the same context and the examine the effects of relaxing the diluteness constraint for rodlike chains. We are currently working on both of these problems.

Acknowledgment is made to the donors of the Petroleum Research Fund, administered by the American Chemical Society, for partial support of this research. We also gratefully acknowledge the financial support of the National Science Foundation Materials Research Laboratory at the University of Massachusetts.

References and Notes

(1) Asakura, S.; Oosawa, F. *J. Chem. Phys.* **1954**, *22*, 1255–1256.
(2) Cooper, A. R. In *Developments in Polymer Characterisation—5*; Dawkins, J. V., Ed.; Elsevier: New York, 1986; pp 131–169.
(3) Barth, H. G. In *Water-Soluble Polymer: Beauty with Performance*; Glass, J. E., Ed.; Advances in Chemistry Series 213; American Chemical Society; Washington, DC, 1986; pp 31–53.
(4) Rollings, J. E.; Bose, A.; Caruthers, J. M.; Tsao, G. T.; Okos, M. R. In *Polymer Characterization: Spectroscopic Chromatographic, and Physical Instrumental Methods*; Craver, C., Ed.; Advances in Chemistry Series 203; American Chemical Society; Washington, DC, 1983; pp 345–358.
(5) Scheutjens, J. M. H. M.; Fleer, G. J. *Adv. Colloid Interface Sci.* **1982**, *16*, 361–379.
(6) Napper, D. H. *Polymeric Stabilization of Colloidal Dispersions*; Academic Press: New York, 1983.
(7) Casassa, E. F. *Macromolecules* **1984**, *17*, 601–604.
(8) Giddings, J. C.; Kucera, E.; Russell, C. P.; Myers, M. N. *J. Phys. Chem.* **1968**, *72*, 4397–4407.
(9) Auvray, L. *J. Phys. (Paris)* **1981**, *42*, 79–95.
(10) Cassassa, E. F. *J. Polym. Sci., Part A-2* **1972**, *10*, 381–384.
(11) Hoagland, D. A. *J. Colloid Interface Sci.* **1988**, *123*, 117–121.
(12) Weigel, F. W. *J. Phys. A* **1977**, *10*, 299–303.
(13) Muthukumar, M. *J. Chem. Phys.* **1987**, *86*, 7230–7234.
(14) Coviello, T.; Kajiwara, K.; Burchard, W.; Dentini, M.; Crescenzi, V. *Macromolecules* **1986**, *19*, 2826–2831.
(15) Manning, G. *J. Chem. Phys.* **1969**, *51*, 924–933.
(16) Fixman, M.; Skolnick, J. *Macromolecules* **1978**, *11*, 863–866.
(17) Russel, W. B. *J. Polym. Sci., Polym. Phys. Ed.* **1982**, *20*, 1233–1247.
(18) Brenner, S. L.; Parsegian, V. A. *Biophys. J.* **1974**, *14*, 327–333.
(19) Stigter, D. *Biopolymers* **1977**, *16*, 1435–1448.
(20) Nicolai, T.; Mandel, M. *Macromolecules* **1989**, *22*, 438–444.
(21) Odijk, T.; Houwaart, A. C. *J. Polym. Sci., Polym. Phys. Ed.* **1978**, *16*, 627–639.
(22) Fixman, M. *J. Chem. Phys.* **1982**, *76*, 6346–6353.
(23) Skolnick, J.; Grimmelmann, E. K. *Macromolecules* **1980**, *13*, 335–338.
(24) Fixman, M. *J. Chem. Phys.* **1979**, *70*, 4995–5004.
(25) Levine, S.; Bell, G. M. *Discuss. Faraday Soc.* **1966**, *42*, 69–79.
(26) Ninham, B. W.; Parsegian, V. A. *J. Theor. Biol.* **1971**, *31*, 405–428.
(27) Brenner, S. L.; McQuarrie, D. A. *J. Colloid Interface Sci.* **1973**, *44*, 298–317.
(28) Ohshima, H. *Colloid Polym. Sci.* **1974**, *252*, 158–164.
(29) Bell, G. M.; Levine, S.; McCartney, L. N. *J. Colloid Interface Sci.* **1970**, *33*, 335–358.
(30) Oshima, H.; Healy, T. W.; White, L. R. *J. Colloid Interface Sci.* **1982**, *90*, 17–26.
(31) James, A. E.; Williams, D. J. A. *J. Colloid Interface Sci.* **1985**, *107*, 44–58.
(32) Hunter, R. J. *Foundations of Colloid Science*; Oxford University Press: New York, 1987; Vol. I.
(33) Tenchov, B.; Brankov, J. G. *J. Colloid Interface Sci.* **1986**, *109*, 172–180.
(34) DiMarzio, E. A.; Guttman, C. M. *Macromolecules* **1970**, *3*, 131–146.
(35) (a) Ausserre, D.; Hervet, H.; Rondelez, F. *Phys. Rev. Lett.* **1985**, *54*, 1948. (b) Rondelez, F.; Ausserre, D.; Hervet, H. *Annu. Rev. Phys. Chem.* **1987**, *38*, 317.
(36) Kim, M. W.; Peiffer, D. G.; Chen, W.; Hsiung, H.; Tasing, Th.; Shen, Y. R. *Macromolecules* **1989**, *22*, 2682–2685.
(37) (a) Smith, F. G., III; Deen, W. M. *J. Colloid Interface Sci.* **1983**, *91*, 571–589. (b) Deen, W. M. *AIChE J.* **1987**, *33*, 1409–1422.
(38) Yau, W. W.; Kirkland, J. J.; Bly, D. D. *Modern Size-Exclusion Liquid Chromatography*; Wiley: New York, 1979.
(39) Manning, G. *J. Chem. Phys.* **1969**, *51*, 924–933.
(40) Davis, R. M.; Russel, W. B. *J. Polym. Sci., Part B: Polym. Phys.* **1986**, *24*, 511–532.
(41) Munch, W. D.; Zestar, L. P.; Anderson, J. L. *J. Membr. Sci.* **1979**, *5*, 77–102.
(42) Smith, F. G., III; Deen, W. M. *J. Colloid Interface Sci.* **1980**, *78*, 444–465.
(43) Deen, W. M.; Smith, F. G., III. *J. Membr. Sci.* **1982**, *12*, 217–237.
(44) Mitchell, B. D.; Deen, W. M. *J. Membr. Sci.* **1984**, *19*, 75–100.
(45) Styring, M. G.; Davison, C. J.; Price, C.; Booth, C. *J. Chem. Soc., Faraday Trans. 1* **1984**, *80*, 3051–3058.
(46) Long, T. D.; Jacobs, D. L.; Anderson, J. L. *J. Membr. Sci.* **1981**, *9*, 13–27.
(47) Le Bret, M.; Zimm, B. H. *Biopolymers* **1984**, *23*, 287–312.